Registration and analysis of laser beam wavefront using a Shack-Hartmann sensor under conditions of artificial pavilion turbulence

V.A. Bogachev[1], M.V. Volkov[1,2], D.E. Guk[1], M.O. Koltygin[1], A.V. Kudryashov[3], R.S. Kuzin[1], A.L. Rukosuev[3], F.A. Starikov[1,2], R.A. Shnyagin[1], A.S. Shtylev[1]

[1] Institute of Laser Physics Research, Russian Federal Nuclear Center – VNIIEF, Sarov, 607188, Russia

[2] Sarov Physics and Technology Institute of NRNU MEPhI, Sarov, 607186 Russia

[3] Institute of Geosphere Dynamics them. Academician M.A. Sadovsky, Moscow, 119334 Russia

ABSTRACT

Using a fast-acting Shack-Hartmann wavefront sensor (WFS) under the conditions of artificially created pavilion turbulence, the possibility of registering and recording the phase front of laser radiation with a high temporal resolution has been experimentally demonstrated. A FPGA has been used as a control element of the WFS that provides an operation frequency of the WFS and recording information about the wavefronts of 4 kHz. Analysis of the reconstructed dynamics of the wavefront of the laser radiation makes it possible to determine in detail various spatiotemporal phase characteristics and to identify non-Kolmogorov features of turbulent distortions.

Keywords: wavefront sensor, atmospheric turbulence, adaptive optics

1. INTRODUCTION

A conventional adaptive optical system, including a wavefront sensor (WFS) and an adaptive mirror, is used for phase correction of optical (including laser) radiation [1]. The WFS is designed to obtain the information about phase distortions and to reconstruct the wavefront that is necessary for subsequent control of the correcting adaptive mirror in the closed loop [2]. But WFS has, in addition, an independent value. Having information on the spatial and temporal distribution of the wavefront registered by WFS, one can obtain estimates of the spatial and temporal parameters of the optically inhomogeneous medium, through which the radiation beam has passed (for example, a turbulent atmosphere). In WFS of Shack-Hartmann type, the determination of the phase surface dynamics and the subsequent analysis of the characteristic parameters of the turbulent medium is based on the knowledge of coordinates of the centers of gravity (centroids) of the focal spots of the hartmanogram [3]. In the case of the Kolmogorov turbulence spectrum it is well known, how atmospheric turbulence affects the spatial and temporal parameters of the wave front radiation. In this connection, it is of particular interest to identify the non-Kolmogorov features of turbulence.

This work is devoted to recording a series of hartmanograms of the wavefront of laser radiation under conditions of artificial pavilion turbulence using a fast Shack-Hartmann WFS [4] and subsequent evaluation of spatial and temporal parameters of turbulence, including the presence of its deviations from the Kolmogorov character. They are concerned with the violation of statistical uniformity and isotropy, the fulfillment of the Taylor hypothesis, the known power dependence of the phase fluctuations in the inertial interval, etc.

2. EXPERIMENTAL SCHEME AND PRIMARY EXPERIMENTAL DATA

Figure 1 shows a schematic of the experiment. The beam of a laser with a wavelength of λ=532 nm is collimated by a telescope (f_1=8 mm and f_2=1.5 m) to a size of D=12 cm. Then the radiation propagates along the path of length L=20 m.

29th International Symposium on Atmospheric and Ocean Optics: Atmospheric Physics,
edited by Oleg A. Romanovskii, Proc. of SPIE Vol. 12780, 127800V
 · 0277-786X · doi: 10.1117/12.2690304

As an artificial source of turbulent distortion in the first case has been used one fan F1 with blade size about 10 cm with vertically directed transverse air flow, in the second case - two identical fans F1 and F2 with crossed transverse air flows, spaced along the beam propagation axis. Then the radiation distorted by turbulent air flow through the telescope of the registration system consisting of a parabolic mirror f_3=1.5 m and a matching lens f_4=50 mm is delivered to the Shack-Hartmann WFS for registration of series of hartmannograms, their processing (determination of centroid matrices) and their saving in computer memory.

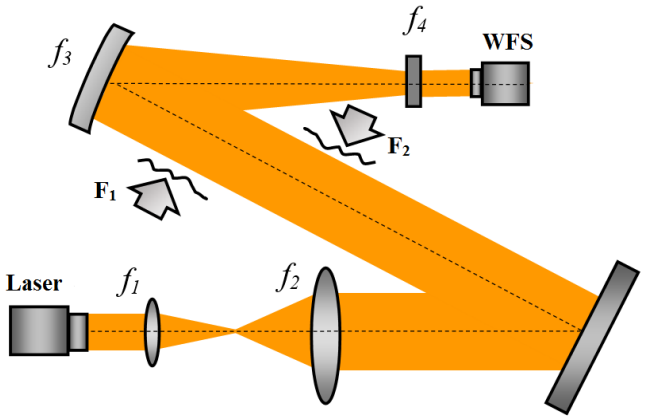

Figure 1. Schematic diagram of the experiment on registration of hartmanograms.

The spatial resolution of the obtained wavefronts is fixed and limited by the size of the subaperture of the WFS. The higher the temporal resolution, the greater the detail of the wavefront features can be studied. The exposure time of the frame in the experiment is 10 μs. It is worth noting that the use of a personal computer to control the WFS imposes significant limitations from above on the frequency of the WFS. Obviously, the images of halftone hartmannograms on the full field of the CCD camera occupy a sufficiently large amount of computer memory and cannot be recorded with a high frequency. Of course, the matrix of centroids (coordinates of centers of gravity of spots of the hartmanogram) occupies significantly less memory and can be recorded at high frequency, but here, again, it is necessary to determine this matrix by processing the whole hartmannogram at each cycle of the WFS operation that again requires significant time.

Therefore, in the present work, a programmable logic integrated circuit, in particular, one of its varieties - a field-programmable gate array (FPGA) with special software "written" into it [4], is used to control the WFS to increase the operation speed. This makes it possible to achieve a frequency of WFS operation equaled to the CCD camera frame rate 4 kHz, and at such a frequency to have time to process hartmanograms, calculate centroid matrices (i.e. local wavefront tip-tilts) and write them into the computer memory. The parameters of the Shack-Hartman WFS are presented in Table 1.

Having a set of hartmanograms recorded at high frequency, it is possible to reconstruct wave fronts of radiation and study their various dynamic, spatial and spectral characteristics in the post-processing mode.

Table 1. Parameters of WFS

Spectral range	350 - 1100 nm
Dynamic range (angles)	± 50 λ
Phase measurement accuracy (PV)	$\lambda/50$
Frame frequency of CCD camera under resolution	2400 fps @ 1920x1080 pix. 4000 fps @ 480x480 pix.
Interface	Optical fiber, 40 Gbit/s
Focal length of lenslet raster *f*	12 mm
Number of working subapertures	20x20
Subaperture size *d*	240 μm
Pixel size Δ	10 μm
Aperture size of input beam	4.8x4.8 mm

The typical hartmanograms recorded under various conditions are shown in Figure 2.

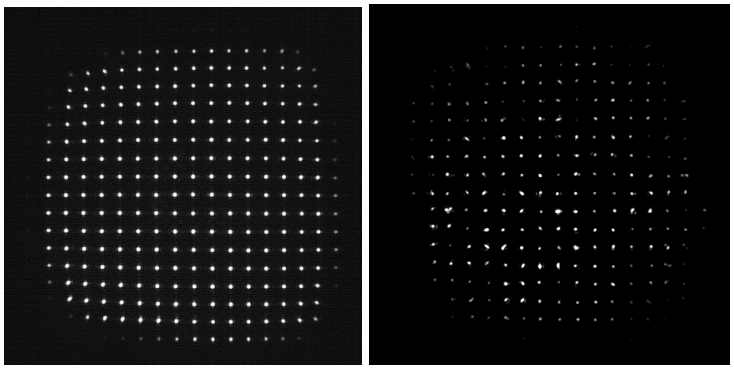

Figure 2. Examples of hartmannograms.

Figures 3 and 4 show the fragments of centroid dynamics in two sub-apertures (central and peripheral) at registration frequency 4 kHz and after application of a filter of frequencies above 400 Hz and 800 Hz for a case of one and two fans accordingly (why such filters were chosen will be clear below). Figure 5 shows the centroid dynamics in the center sub-aperture after applying a filter below 400 Hz and 800 Hz for the case of one and two fans, respectively. From Figures 3 and 4 we can see that the signal of the primary experimental information experiences temporal fluctuations with the amplitude up to a few hundredths of a pixel size Δ. Obviously, this value is associated with an error in determining the coordinates of the centroid at a finite number of pixels in the subaperture (6÷8), which the spot occupies, as well as with insufficient local spatial resolution. Figure 5 shows that this error does not exceed Δ/20. Therefore, the accuracy of the local phase measurement is not worse than $(kd/f)(\Delta/20) = 2\pi/(20\lambda f/d\Delta) = 2\pi/55$ rad. As for the RMS phase measurement error, the calculation based on Figure 5 gives 2π/300÷2π/250, i.e. about 5 times less.

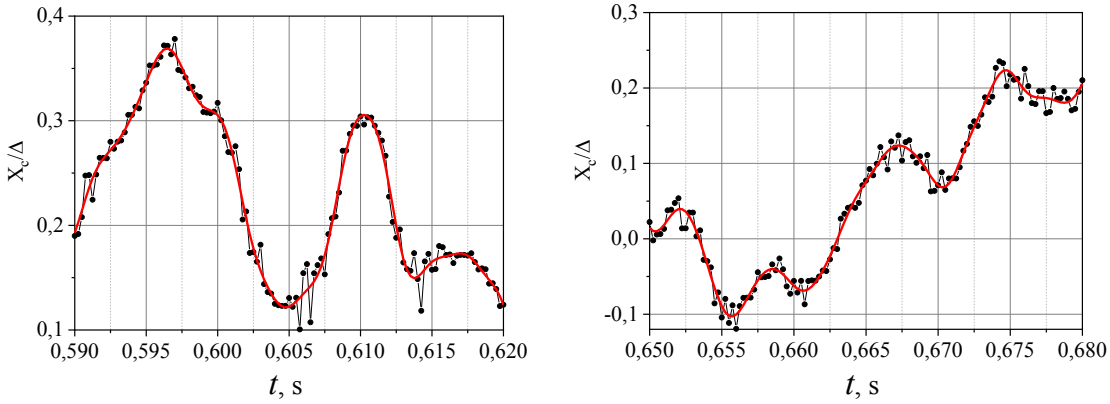

Figure 3. Dynamics of centroid fluctuations in the central (left) and peripheral (right) subapertures at the registration frequency of 4 kHz (markers) and after applying a frequency filter above 400 Hz (red line) when turbulence is created by a single air flow

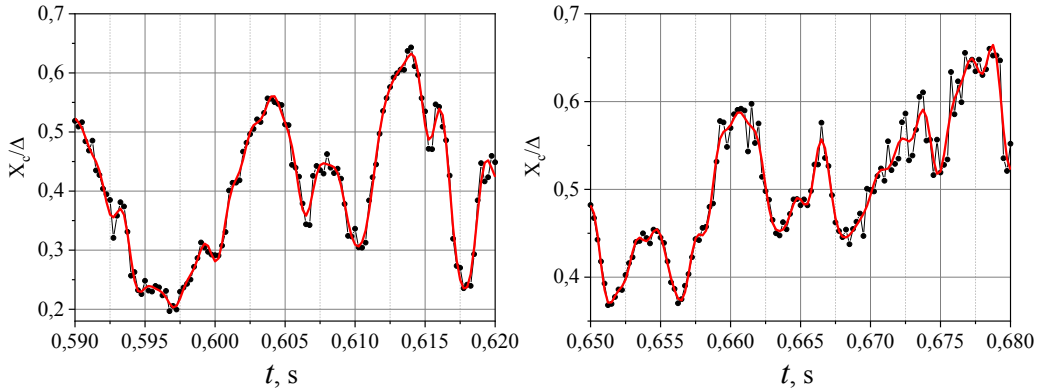

Figure 4. Dynamics of centroid fluctuations in the central (left) and peripheral (right) subapertures at the registration frequency of 4 kHz (markers) and after application of a frequency filter above 800 Hz (red line), when turbulence is created by two air flows

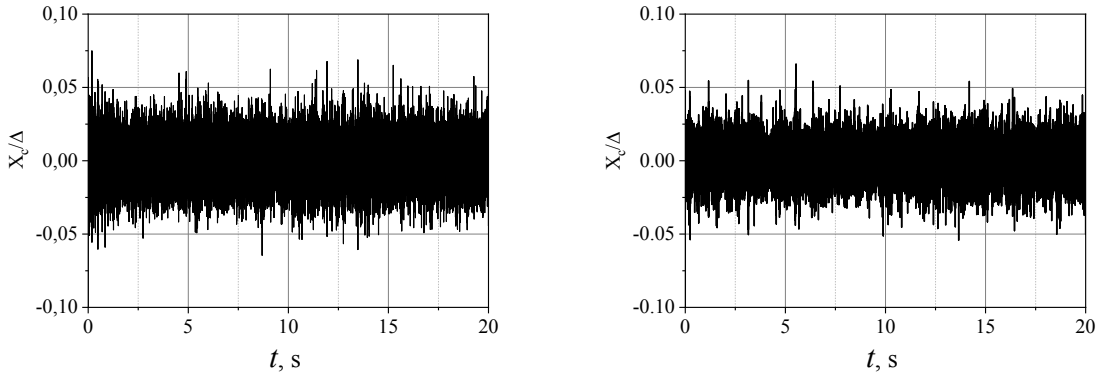

Figure 5. Dynamics of high-frequency centroid fluctuations in the central subaperture after applying a frequency filter below 400 Hz (left), when turbulence is created by one airflow, and above 800 Hz (right), when turbulence is created by two airflows

The coherence radius (in the free atmosphere, it would be the Fried radius) can serve as a spatial characteristic of wavefront inhomogeneities. To determine the radius of coherence of radiation using the Shack-Hartmann WFS, we used a method [5] based on measuring the difference in the angles of the radiation wavefront slope at the WFS subapertures, naturally, assuming the Kolmogorov character of turbulence. The calculation has shown that in the case of single fan, the coherence radius takes a value of ~2.2 cm, and in the case of two crossed fans ~ 2.0 cm. In our case, the size of the subaperture of the WFS in terms of the full beam aperture is s=0.7 cm (taking into account the scaling), which provides the required spatial resolution: the size of the subaperture should not be larger than the coherence radius [6].

3. SPATIAL CHARACTERISTICS OF WAVEFRONT

For reconstructing the wavefront of the laser beam, Fried's discretization scheme [7] has been used. Figure 6 shows the temporal evolution of the reconstructed wave fronts of the laser radiation when turbulence has been created by one fan. Figure 7 shows similar patterns when turbulence was created by two crossed fans.

Figures 6 and 7 do not show a clear "wind" drift of the phase front, which has been observed in [4] and which would clearly confirm the fulfillment of the Taylor hypothesis. This is apparently due to the fact that the size of the fan blade is less than the laser beam aperture of 12 cm that caused noticeable mixing of the air within the beam aperture.

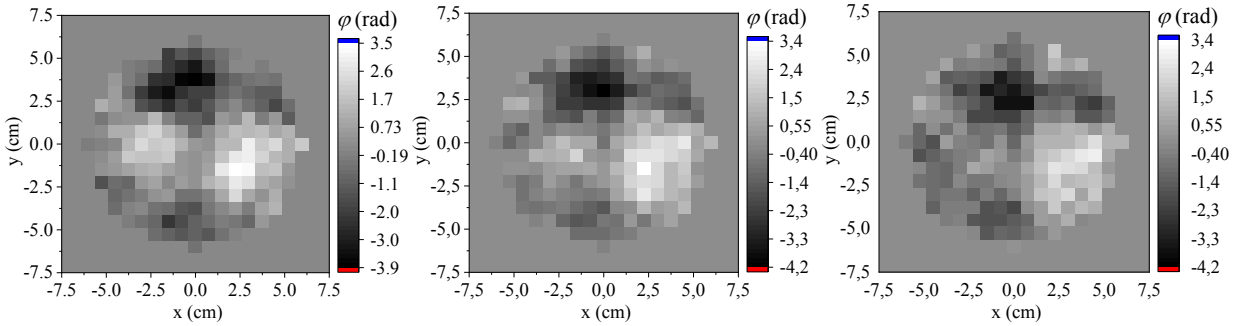

а) t=10 ms б) t=20 ms в) t=30 ms

Figure 6. Temporal evolution of the reconstructed wavefronts when turbulence is created by one airflow

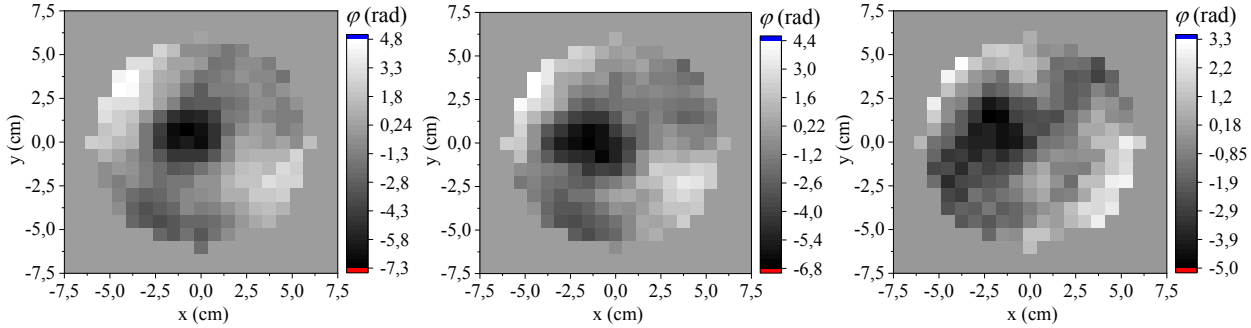

а) t=130 ms б) t=260 ms в) t=390 ms

Figure 7. Temporal evolution of the reconstructed wave fronts when turbulence is created by two crossed airflows

According to the classical definition [8], the coherence radius for Kolmogorov turbulence is the size of the aperture, at which the dispersion of phase fluctuations reaches 1 rad^2. Figure 8 shows the calculated dependence of the phase dispersion against the aperture size. This dependence is averaged over the entire time interval of the hartmannogram registration of 20 sec.

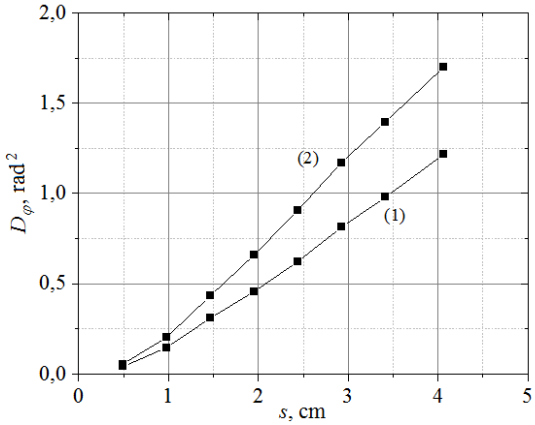

Figure 8. Dependence of phase dispersion when turbulence is created by one flow (1) and two air flows (2)

As can be seen from Figure 8, in the case of one fan the coherence radius takes the value ~ 3.5 cm, and in the case of two crossed fans it is equal to ~ 2.6 cm. These values of the coherence radius differ from the values (2.2 cm and 2.0 cm, respectively) obtained from the analysis of the difference in the angles of the wave front slope of the radiation at the subapertures of the WFS under the assumption of Kolmogorov turbulence statistics. A possible reason for this is that the use of the Kolmogorov formalism in calculating the coherence radius in conditions where non-Kolmogorov turbulence features are significant is unreasonable.

4. TEMPORAL CHARACTERISTICS OF WAVEFRONTS

Let us move on to the dynamic characteristics of the wavefront. Figure 9 shows the phase dynamics in the central subaperture of the WFS obtained at the registration frequency of 4 kHz. In the peripheral subapertures of the WFS, as the experiment showed, the situation is similar.

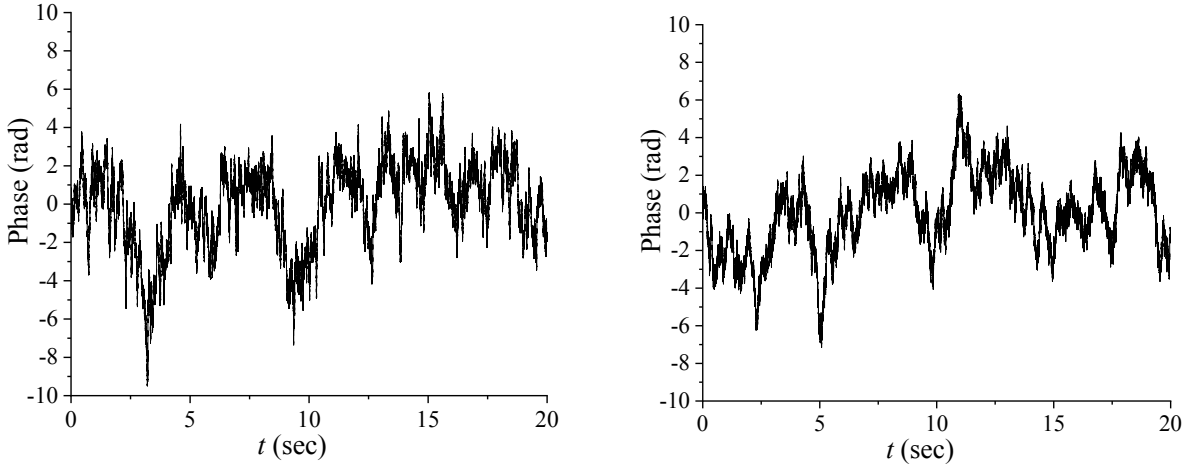

Figure 9. Phase dynamics in the central subaperture of the WFS when turbulence is created by one flow (left) and two crossed airflows (right)

Figure 10 shows the spectral power of local phase fluctuations in the central subaperture of the WFS, associated with the Fourier transform from the time dependences in Figure 9. It extends up to a frequency of 2 kHz in agreement with the 4 kHz working frequency of the WFS. The power dependence $\sim \nu^{-8/3}$, characteristic of the inertial interval of the Kolmogorov turbulence [8], is shown in Figure 10 by a sloping straight line. As it can be seen from Figure 10, the spectrum of artificial turbulence in our case differs from the Kolmogorov one. It decays according to a power law, slower (rather $\sim \nu^{-5/3}$) and completely uncharacteristic of coherent turbulence [9, 10], where there is a faster decay of the spectrum, $\sim \nu^{-11/3}$. This confirms the above conclusion about the presence of significant non-Kolmogorov features of the artificial turbulence created and, in addition, suggests a variety of possible violations of the Kolmogorov law.

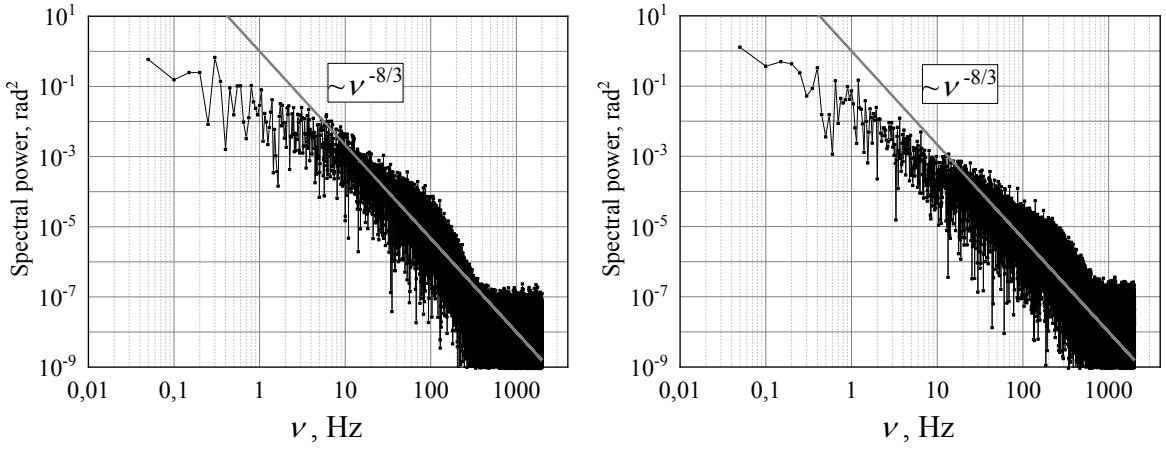

Figure10. Spectral power of phase fluctuations in the central subaperture of the WFS when turbulence is created by one flow (left) and two crossed air flows (right)

Note that at high frequencies in the spectrum of phase fluctuations in Figure 10 there is a kink, when the phase begins to decrease according to the law faster than $\nu^{-8/3}$. In the case of turbulence created by the air flow from one fan, the break begins at a frequency of about 100 Hz, in the case of two cross-flows - at a frequency of about 250 Hz. This is due to the

fact that phase inhomogeneities, the scale of which is smaller than the size of the WFS subaperture, give a significantly smaller contribution to the local phase tip-tilts. Within the framework of the Kolmogorov model and fulfillment of the Taylor hypothesis, the frequency at which the above kink is observed is determined by the ratio of the weighted mean wind speed υ to the size of the subaperture of the WFS s [8]. From this we can estimate the value of the weighted average wind speed υ, in the first case $\upsilon \approx 0.7$ m/s, in the second $\upsilon \approx 1.7$ m/s (of course, do not forget that the estimate assumes the implementation of the Taylor hypothesis).

Further, as can be seen from Figure 10, starting from a frequency of about 400 Hz in the case of one fan and 800 Hz in the case of two fans there is a noise "sole" in the spectrum. The spectral level of the "sole" is about the same. The difference of frequencies, from which the "sole" is observed, is explained by the fact, that in case of two fans the spectral power level of high-frequency harmonics is higher, than in case of one fan.

Figure 11 shows the absolute and normalized integrals from the spectral power of phase fluctuations by frequency in the two described cases.

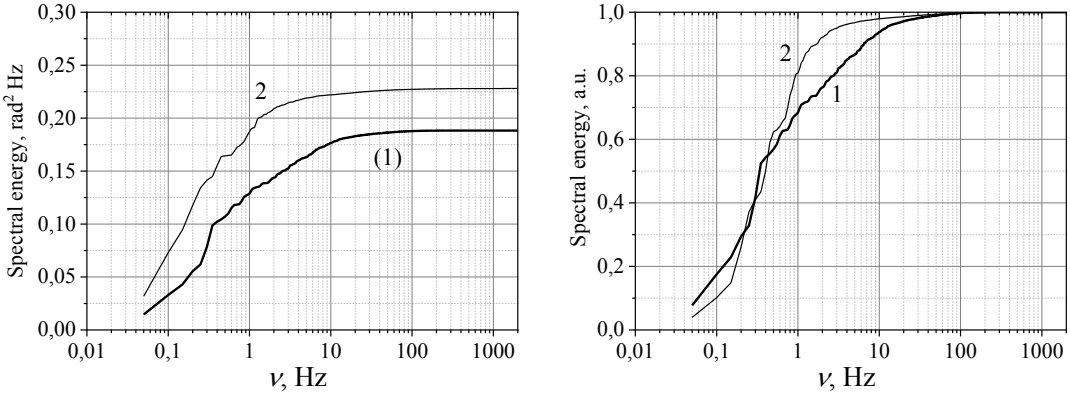

a) b)

Figure 11. Absolute (a) and normalized (b) integrals from the spectral power of phase fluctuations in the case of one flow (curve 1) and two air flows (curve 2)

It follows from Figure 11a that the “energy” of turbulence in the case of two crossed air flows exceeds the “energy” of turbulence in the case of one air flow that should be expected. However, according to Figure 11b, in the frequency range from 1 Hz to 10 Hz, the relative contribution to the “energy” of turbulence is smaller in the case of two air streams. Higher frequencies do not make a significant contribution - practically all “energy” of turbulence is contained in the band up to ~ 100 Hz in both cases. Also note that the spectral "sole" does not contribute to the "energy" of turbulence, i.e., the presence of noise does not affect the meaningful results.

Figure12 shows the dynamics of high-frequency phase component after filtering the frequencies below 400 Hz in case of one fan and 800 Hz in case of two fans. It can be seen that the amplitude of phase noise does not exceed 0.1÷0.2 rad (by RMS 0.03÷0.04 rad), i.e. the accuracy of local phase determination is $2\pi/60 \div 2\pi/30$ (by RMS $2\pi/220 \div 2\pi/150$), which agrees with the accuracy estimate obtained in section 2 based on the analysis of wavefront slopes (Figures 3-5).

Figures 13 and 14 show the spectral power of local phase fluctuations obtained after averaging the original series of hartmanograms over 4 and 20 frames. This corresponds to a WFS operating frequency of 1 kHz and 200 Hz; the spectrum extends to a frequency of 500 Hz and 100 Hz, respectively. Comparison of Figures 13 and 14 with Figure 10 shows that averaging did not lead to a deformation of the spectral distribution, including the "sole". This means that the fast response of the WFS is redundant in the measurement of wavefronts under consideration. Naturally, if there are high-frequency components in the wavefront with an amplitude exceeding the noise amplitude, they would be reliably registered. Formation of such components in our experiments by increasing the fan rotation speed led to a decrease in the coherence radius and a lack of spatial resolution.

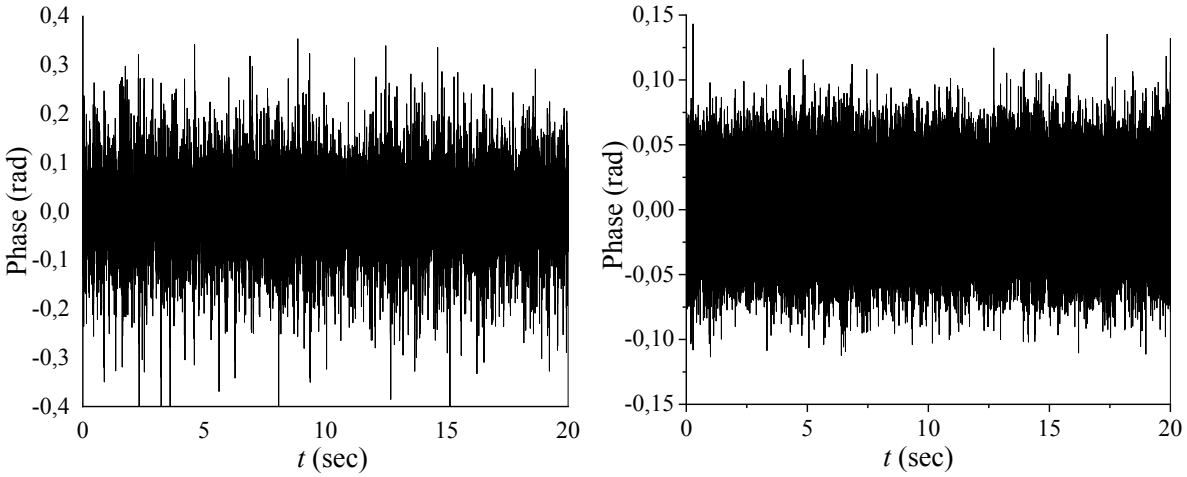

Figure 12. Dynamics of high-frequency phase fluctuations in the central subaperture after applying a frequency filter below 400 Hz (left), when turbulence is created by a single airflow, and below 800 Hz (right), when turbulence is created by two airflows

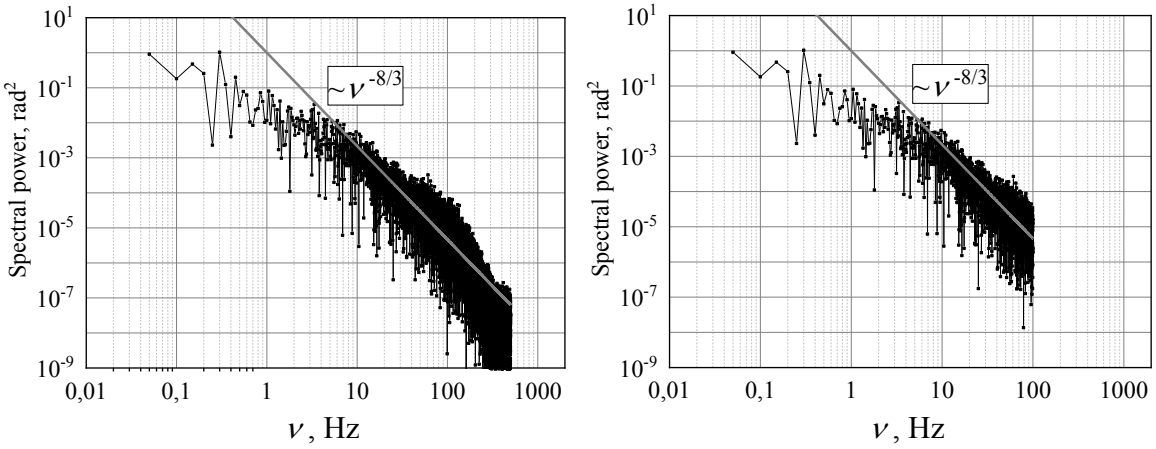

a) b)

Figure 13. Spectral power of phase fluctuations at averaging the hartmannogram series over 4 (a) and 20 (b) frames, when turbulence is created by single air flow

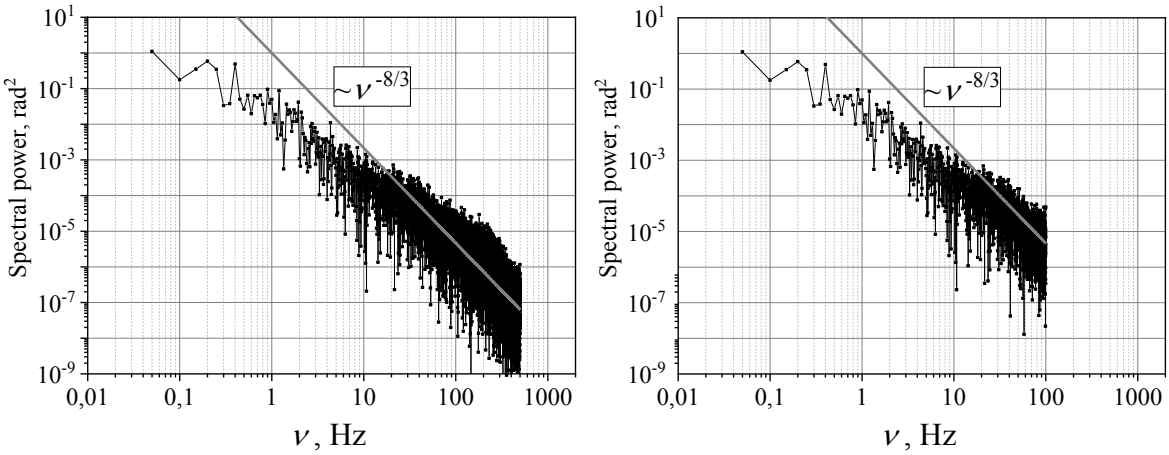

a) b)

Figure 14. Spectral power of phase fluctuations at averaging the hartmannogram series over 4 (a) and 20 (b) frames, when turbulence is created by two air flows

5. CONCLUSIONS

Thus, with the help of the fast-acting Shack-Hartmann wavefront sensor with a clock frequency of 4 kHz, the dynamical wavefront of laser radiation under the conditions of artificial pavilion turbulence has been registered and the possibility of analyzing the spatial and temporal parameters of the phase front for the detection of non-Kolmogorov features of turbulence has been shown. The accuracy of the local phase measurement (PV) by the WFS is at the level of $\lambda/60 \div \lambda/30$.

ACKNOWLEDGMENTS

The research was conducted within the framework the scientific program of the National Center for Physics and Mathematics (project “Physics of High Energy Density. Phase 2023-2025”).

REFERENCES

[1] Tyson R. K. Principles of Adaptive Optics. Boston: Academic, 1998.

[2] Platt B.C., Shack R., *J. of Refractive Surgery* **17**, 573 (2001).

[3] Antoshkin L.V., Lavrinov V.V., Lavrinova L.N., Lukin V.P., Differential method for wavefront sensor measurements of turbulence parameters and wind velocity, *Atmospheric and oceanic optics* **21**, 64-68 (2008).

[4] Rukosuev A.L., Belousov V.N., Nikitin A.N., Sheldakova Yu.V., Kudryashov A.V., Bogachev V.A., Volkov M.V., Garanin S.G., Starikov F.A., “Smart adaptive optical system for the wavefront correction of laser radiation distorted by atmospheric turbulence”, *Quantum electronics* **50**, 707–709 (2020).

[5] Fried D. L. “Differential angle of arrival: theory, evaluation and measurement feasibility”, *Radio Sci.* **10** (1), 71-76 (1975).

[6] Volkov M.V., Bogachev V.A., Starikov F.A., 19th International Conference on Laser Optics “ICLO-2020”, St. Petersburg, Technical Program, WeR4-p12, (2020) [IEEE Proceedings, DOI: 10.1109/ICLO48556.2020.9285761].

[7] Fried D.L., "Least-Square Fitting a Wave-Front Distortion Estimate to an Array of Phase-Difference Measurements," *J. Opt. Soc. Am.* **67**, 370-375 (1977).

[8] Hardy J.W., Adaptive optics for astronomical telescopes. New York: Oxford University press, 1998. 438 p.

[9] Nosov V. V., Lukin V. P., Kovadlo P. G., Nosov E. V., Torgaev A. V., “Intermittency of Kolmogorov and coherent turbulence in the mountain atmospheric boundary layer (Review)”, *Atmospheric and oceanic optics* **35**, 266-287 (2022).

[10] Nosov V.V., Lukin V.P., Kovadlo P.G., Nosov E.V., Torgaev A.V., “Proof of Hopf's conjecture on the structure of turbulence (Tatarsky's memory)”, *Optika atmosfery i okeana* **36**, 12-18 (2023) (in Russian).